Low-order aberration sensitivity of an optical vortex coronagraph

David M. Palacios and Sarah L. Hunyadi

Jet Propulsion Laboratory, California Institute of Technology, 4800 Oak Grove Drive, Pasadena, California 91109

Received June 2, 2006; accepted June 5, 2006;
posted July 25, 2006 (Doc. ID 67061); published September 25, 2006

We describe a high-contrast imaging technique capable of directly measuring light from a terrestrial planet by using a vortex mask of topological charge $m=5$. We demonstrate that this technique is relatively insensitive to low-order aberrations and compare its performance to that of a band-limited Lyot coronagraph.

OCIS codes: 050.1970, 350.1260, 350.6090, 070.6110, 110.6770.

The imaging of exosolar planets is one of the top priorities in astronomy. However, searching for exosolar terrestrial planets in visible light presents a daunting task, requiring the stellar light to be reduced by a factor of 10^{-10}! Several starlight suppression devices, such as stellar coronagraphs, have been investigated to achieve this high level of contrast.[1–4] Stellar coronagraphs employ an image-plane occulting mask to preferentially obstruct starlight, enhancing the contrast between the star and nearby objects (e.g., planets). There are two basic types of image-plane occulting masks: amplitude masks and phase masks. Ideally, an amplitude mask attenuates the on-axis starlight in the image plane without significantly attenuating the light from an off-axis source. Band-limited masks are a special type of amplitude mask with a frequency domain representation that is nonzero only for a finite band of spatial frequencies.[5] Trauger *et al.*[6] used a band-limited mask to demonstrate the deepest light suppression to date ($\sim 10^{-9}$). It is also possible to attenuate starlight with a phase mask, which reduces starlight by phase shifting two or more regions of the stellar wave front by π rad, thus creating an interference null in the stellar intensity profile.[7]

In this Letter we examine the performance of a new type of high-contrast coronagraph, known as an optical vortex coronagraph[8] (OVC). An optical vortex may be characterized as a dark core of destructive interference produced by a helical phase defect in a beam of spatially coherent light. A scalar beam of light with a centrally embedded optical vortex may be described in cylindrical coordinates (ρ,ϕ,z) by the field[9]

$$E(\rho,\phi,z,t) = A(\rho,z)\exp(im\phi)\exp(i\omega t - ikz), \quad (1)$$

where $A(\rho,z)$ is a circularly symmetric amplitude function, $\omega = 2\pi c/\lambda$ is the angular frequency of a monochromatic field of wavelength λ, $k = 2\pi/\lambda$ is the wavenumber of the field, and m is the topological charge. The light beam described by Eq. (1) is said to possess vorticity because at any fixed instant of time helical surfaces given by $m\phi - kz = \text{constant}$ are produced for integer values of m. In addition, the amplitude vanishes along the helix axis ($\rho = 0$) forming a dark central core that persists for all values of z, i.e., $A(0,z) = 0$.

A monochromatic, planar ($m = 0$) beam may be converted into a vortex beam by transmitting the light through a transparent diffractive phase mask.[10] Light passing through the mask gains an azimuthally varying phase pattern and an amplitude profile containing an embedded dark core, which may be used to attenuate a coherent beam of light.[11] After attenuation, a mutually incoherent background signal may be detected,[12] which is the basis of an OVC.

A simple OVC architecture is depicted in Fig. 1. Light from an unresolved star is imaged by L_1, which represents the telescope optics. A vortex mask (OVM) is placed near the focus of L_1, creating a dark central null in the beam. Lens L_2 then collimates the beam, which subsequently passes through a Lyot stop. The Lyot stop blocks the unwanted, on-axis starlight, and the remaining light is reimaged by L_3, allowing the detection of nearby faint objects (e.g., planets).

In an actual coronagraph system the optical surfaces are slightly distorted, creating aberrations that deform the vortex core. This allows light to leak past the Lyot stop, reducing the performance of the coronagraph (i.e., starlight attenuation). One performance evaluation criterion is the contrast sensitivity of the coronagraph to low-order wavefront aberrations.[13] Contrast may be defined as the ratio of

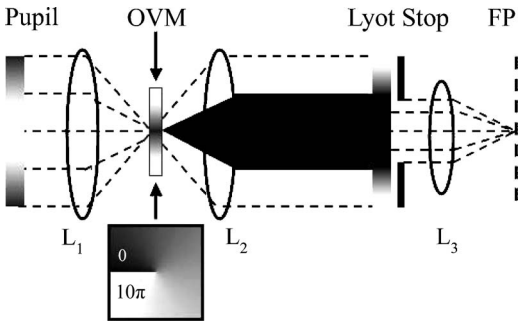

Fig. 1. Simple unfolded model of an optical vortex coronagraph. Lens (L_1) represents the telescope optics, which focus the light from the entrance pupil onto an $m=5$ optical vortex mask (OVM). The inset depicts the OVM phase profile. Lens (L_2) collimates the light forming an exit pupil where we place a Lyot stop. A third lens (L_3) reimages the light to the final focal plane at (FP).

0146-9592/06/202981-3/$15.00

the intensity in the final image plane when the occulter is in place to the intensity when the occulter is removed. As a way of further simplifying the comparison of different coronagraphs, Green and Shaklan[13] evaluated the average contrast over a ring located at $\rho_0 = 4\lambda f/D$, where D is the diameter of the entrance pupil and f is the focal length of the imaging lens (L_1 in Fig. 1). The average contrast evaluated at $\rho = \rho_0$ is given by[14]

$$\bar{C}_{\rho_0} = (1/A_R)\int_0^{2\pi} I(\rho_0,\phi)/\{I_{\text{open}}(\rho_0,\phi)|o(\rho_0,\phi)|^2\}\mathrm{d}\phi, \tag{2}$$

where A_R is the integration area of the ring located at ρ_0, $I(\rho_0,\phi)$ is the intensity in the final image plane (FP in Fig. 1) when the mask is in place, $I_{\text{open}}(\rho_0,\phi)$ is the intensity in the final image plane when the mask is removed, and $o(\rho,\phi)$ is the occulting mask transmission function. The contrast sensitivity of a coronagraph may be obtained by fitting the curve of $\bar{C}_{\rho_0}$ versus aberration size to a power law given by $\bar{C}_{\rho_0} = \alpha + \beta\Delta^{\gamma}$, where α is the contrast of the unaberrated system, β is a scaling factor determined from the least-squares fit, Δ is the size of the aberration, and γ is the order of the contrast sensitivity. In an ideal coronagraph, the occulting mask filters out aberrations that have a power-law dependence less than γ. In theory, the linear sinc^2 mask used by Trauger *et al.*[6] possessed a fourth-order contrast sensitivity, and amplitude masks exhibiting an eighth-order contrast sensitivity are under investigation.[16,17] As we will show, an OVC theoretically has a $2m$th-order contrast sensitivity, implying that a vortex mask of charge $m > 4$ will have lower contrast sensitivity than the previously mentioned amplitude masks.

By using a simple analytic model based on the architecture depicted in Fig. 1, it is possible to derive the approximate contrast sensitivity of an OVC. We assume the entrance pupil has a uniform amplitude transmission function, $P(r)$, and a phase transmission function $\Phi(r,\theta) \ll 1$, where (r,θ) denote the pupil plane coordinates. Therefore, the complex field at the entrance pupil may be approximated as

$$E(r,\theta) = P(r)\left[1 + \sum_{l=1,2,3\ldots}\frac{i^l}{l!}\Phi(r,\theta)\right]. \tag{3}$$

In this case, $P(r) = 1$ inside the pupil, and $P(r) = 0$ outside of the pupil. If a vortex mask is placed near the focus of L_1 (see Fig. 1), the focal plane field is given by $E(\rho,\phi) = \mathrm{FT}\{E(r,\theta)\}M(\rho)\exp(im\theta)$, where (ρ,ϕ) denotes the image plane coordinates, $\mathrm{FT}\{E(r,\theta)\}$ is the two-dimensional Fourier transform of $E(r,\theta)$, and $M(\rho)$ is the amplitude transmission function of the vortex mask. The beam is then collimated by lens L_2 (see Fig. 1), and the reimaged pupil, $P_{\text{exit}}(r,\theta)$, may be represented by the convolution of $E(r,\theta)$ with $\mathrm{FT}\{M(\rho)\exp(im\phi)\}$. The vortex mask amplitude transmission function may be approximated as[15]

$$M(\rho) = \tanh^m(\rho/w_v), \tag{4}$$

where w_v is the vortex core waist size. By expanding Eq. (4) in a Taylor's series about $\rho = 0$, $M(\rho)$ is given by

$$M(\rho) \approx \sum_{k=1,2,3\ldots} a_k\rho^k, \qquad a_k = (1/w_v k!)\left[\frac{\partial^k}{\partial\rho^k}M(\rho=0)\right]. \tag{5}$$

The derivatives in relation (5) are zero for $k < m$, implying that $k = m$ is the first nonzero term. By utilizing relation (5) and converting $\mathrm{FT}\{M(\rho)\exp(im\phi)\}$ into a Hankel transform, $P_{\text{exit}}(r,\theta)$ may be represented as

$$P_{\text{exit}}(r,\theta) = E(r,\theta)\sum_{k=m,m+1,m+2\ldots} a_k H_m\{\rho^k\}\exp(im\theta), \tag{6}$$

where $H_m\{f(\rho)\}$ represents the mth-order Hankel transform of $f(\rho)$. Substituting Eq. (3) into Eq. (6) and evaluating the Hankel transform[18] yields

$$\begin{aligned} P_{\text{exit}}(r,\theta) = P(r)&\left(1 + \sum_{l=1,2,3\ldots}\frac{i^l}{l!}\Phi^l(r,\theta)\right) \\ &\times \sum_{k=m,m+1,m+2\ldots} a_k\left(\frac{-1}{2\pi}\right)^k r^{m-k}\frac{\mathrm{d}^k}{\mathrm{d}r^k} \\ &\times\left[\frac{1}{r^{m-k}}\delta(r)\right]\exp(im\theta). \end{aligned} \tag{7}$$

The coronagraph leakage due to the first term in the expansion of the phase aberration [$k = m$, $l = 1$ in Eq. (7)] is proportional to the mth derivative of the phase aberration. Therefore all phase aberrations with a radial dependence of less than m will not contribute to the coronagraph leakage, and an OVC will exhibit an mth-order sensitivity in amplitude. Since contrast is proportional to intensity, we predict that an OVC will possess a $2m$th-order contrast sensitivity.

To verify this prediction, we simulated the performance of an OVC with an entrance pupil diameter of $D = 1000$ pixels, a Lyot stop diameter of $D_L = 0.52D$, and an $m = 5$ vortex mask designed for $\lambda_0 = 550$ nm with $w_v = 0.014D$. An $m = 5$ vortex mask was chosen to maximize the order of the sensitivity while still adhering to current manufacturing limitations (single spiral masks of charge $m \geq 6$ are not currently possible). In addition, the value of w_v was chosen to best simulate the nonideal amplitude transmission of a slightly defocused vortex mask but was small enough not to affect the average contrast at $\rho = \rho_0$. Furthermore, we assumed that the focal plane profile incident on the vortex mask was an ideal Airy profile.[18]

The performance of an OVC was measured by applying small wavefront perturbations, represented by the first 12 Noll ordered Zernike polynomials,[19] to the entrance pupil of the system (located at L_1 in Fig. 1). The resulting average contrast at $\rho = \rho_0$ was then computed using Eq. (2) and plotted versus the peak-to-valley aberration size (see Fig. 2). The contrast

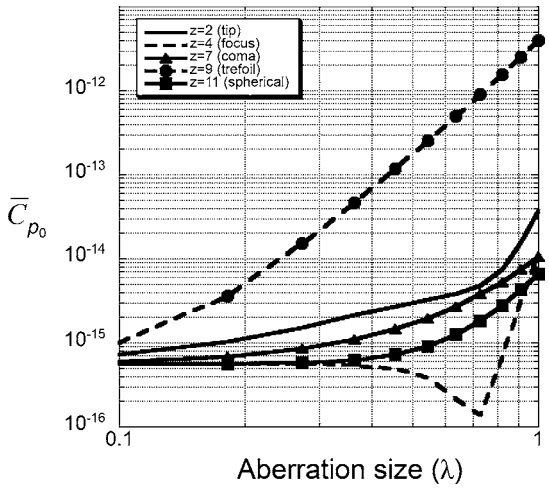

Fig. 2. Plots of contrast versus aberration size (waves peak to valley) depicting the aberration sensitivity of an $m=5$ vortex coronagraph to various Noll ordered Zernike polynomials (z). This is evaluated as the average contrast at a $4\lambda/D$ annulus around a star.

Table 1. Comparison of Aberration Sensitivities to z^a

	z										
	2	3	4	5	6	7	8	9	10	11	12
Eighth-order mask	8	8	4	4	4	4	4	4	4	2	2
$m=5$ OVC	9	9	—	6	6	4	4	5	5	5	5

[a]A linear eighth-order mask is compared with an $m=5$ vortex coronagraph (OVC); z is the Noll ordered Zernike polynomial. For the OVC there is no value for $z=4$ because no accurate estimate could be obtained from the irregular plot (Fig. 2).

sensitivity of an OVC was determined by fitting each plot to a power law by the method of least squares. The values of the fitted power-law exponent, γ, as well as the simulated γ values obtained by Shaklan and Green for a linear eighth-order mask,[17] are listed in Table 1. The $m=5$ OVC demonstrated ninth-order contrast sensitivity to tip–tilt ($z=2$, $z=3$) but did not yield the predicted tenth-order sensitivity. This departure from the theoretical model is due to higher-order terms ($l>1$) in Eq. (7). Even with this departure from the predicted sensitivity, the $m=5$ OVC demonstrated a lower contrast sensitivity than a linear eighth-order mask. It should also be noted that the OVC throughput for a planet, located at an angular position of $4\lambda/D$ away from its parent star, was approximately equal to the throughput reported by Shaklan and Green[16] for the optimized linear eighth-order coronagraph. However, since we obtain high contrast with the OVC, a larger Lyot stop could be used, increasing the planet light throughput.

In this Letter we addressed the optimization of the low-order aberration sensitivity of an OVC. An OVC may hold several key advantages for terrestrial planet detection. Low aberration sensitivity, high planet light throughput, and potential broadband operation[20] are just a few of the key advantages. Other uses of a high-contrast OVC might include sensor protection, characterization of exozodiacal dust, enhanced resolution of binary star systems, and improved edge detection in optical coherence tomography. Future work will address the optimization of other performance criterion such as the inner working angle and planet light throughput.

We thank G. A. Swartzlander, Jr., for many helpful discussions on optical vortices. We also thank S. Shaklan and J. Green for their suggestions and comments. D. M. Palacios' e-mail address is David.M.Palacios@jpl.nasa.gov.

References

1. M. B. Lyot, Mon. Not. R. Astron. Soc. **99**, 578 (1939).
2. N. J. Kasdin, R. J. Vanderbei, D. N. Spergel, and M. G. Littman, Astrophys. J. **582**, 1147 (2003).
3. J. R. P. Angel, Nature **368**, 203 (1994).
4. O. Guyon, Astron. Astrophys. **404**, 379 (2003).
5. M. J. Kuchner, and W. A. Traub, Astrophys. J. **570**, 900 (2002).
6. J. T. Trauger, C. Burrows, B. Gordon, J. J. Green, A. E. Lowman, D. Moody, A. F. Niessner, F. Shi, and D. Wilson, in Proc. SPIE **5487**, 1330 (2004).
7. D. Rouan, P. Riaud, A. Boccaletti, Y. Clenet, and A. Labeyrie, Publ. Astron. Soc. Pac. **112**, 1479 (2000).
8. G. Foo, D. M. Palacios, and G. A. Swartzlander, Jr., Opt. Lett. **30**, 3308 (2005).
9. M. Vasnetsov and K. Staliunas, eds., *Optical Vortices*, Vol. 228 of Horizons in World Physics (Nova Science, 1999).
10. F. B. Colstoun, G. Khitrova, A. V. Fedorov, T. R. Nelson, C. Lowery, T. M. Brennan, B. G. Hammons, and P. D. Maker, Chaos, Solitons Fractals **4**, 1575 (1995).
11. G. A. Swartzlander, Jr., Opt. Lett. **26**, 497 (2001).
12. D. Palacios, D. Rozas, and G. A. Swartzlander Jr., Phys. Rev. Lett. **88**, 103902 (2002).
13. J. J. Green and S. B. Shaklan, in Proc. SPIE **5170**, 25 (2003).
14. We have derived Eq. (2) by evaluating Eq. (12) of Ref. 15 over a set of field points, $\chi_n=1$, for each field point in the final image plane.
15. Z. S. Sacks, D. Rozas, and G. A. Swartzlander, Jr., J. Opt. Soc. Am. B **15**, 2226 (1998).
16. M. J. Kuchner, J. Crepp, and J. Ge, APJ **628**, 466 (2005).
17. S. B. Shaklan and J. J. Green, APJ **628**, 474 (2005).
18. J. D. Gaskill, *Linear Systems, Fourier Transforms, and Optics* (Wiley, 1978).
19. R. J. Noll, J. Opt. Soc. Am. **66**, 207 (1976).
20. G. A. Swartzlander, Jr., Opt. Lett. **30**, 2876 (2005).